5th ECPMG Delft · 2024

Proceedings of the 5th ECPMG 2024
5th European Conference on Physical Modelling in Geotechnics
2-4 October 2024, Delft, the Netherlands

Investigation of tunnel-ground interaction at weak zone during seismic loading: a research using 2D shaking table apparatus and corresponding numerical analysis

Y. Cui
Department of Engineering, Yokohama National University, Yokohama, JP, sai-ei-mx@ynu.ac.jp

S. Ahmed
Shimizu Corporation, Tokyo, J.P., ahmed_s@shimz.co.jp

M. Manuit
Department of Public Works and Highways-Cordillera Administrative Region, Baguio City, PH, manuit.mikael@dpwh.gov.ph

M.O. Ciantia
School of Science and Engineering, University of Dundee, Dundee, Scotland, UK, m.o.ciantia@dundee.ac.uk
Department of Earth and Environmental Sciences, University of Milano Bicocca, Milan, IT, matteo.ciantia@unimib.it

ABSTRACT: Weak areas adjacent to tunnel linings may emerge during or post-construction due to various factors, including substandard quality, water erosion, and dynamic loading. This research visually scrutinized the seismic response of the lining and the surrounding ground by employing a two-dimensional (2D) shaking table apparatus and assessing the influence of weak zones on tunnel integrity. The experimental setup used aluminium rods to replicate sandy ground conditions, and the weak zone was modelled by increasing the void ratio of the ground. The strain of the tunnel lining and the displacement of the surrounding ground were analyzed throughout the shaking process. Experimental findings revealed significant variations in ground movement and notable fluctuations in lining deformation, with observed quantities heavily reliant on the location of the weak zone. The volumetric strain variation indicates the lining can not observe enough reaction from the backside ground when weak zones exist, resulting in a heightened bending moment on the lining at this weak area. These observations underscore the potential for even minor weak zones to induce substantial damage to tunnel linings during seismic events. This paper presents the findings of the 2D shaking table test alongside corresponding numerical analyses, elucidating the dynamics of tunnel-ground interaction in the presence of weak zones during seismic loading.

1 GUIDELINES

Tunnels constitute critical underground infrastructure, necessitating the maintenance of high safety standards under both static and dynamic loads. However, weak zones may develop around tunnels due to various factors such as poor workmanship, inadequate backfilling of supporting material, water erosion, and dynamic loads induced by construction activities (Howard, 1991; Meguid and Dang, 2009; Gomes et al., 2015; Zhang et al., 2019). The characteristics of the weak zone manifest as cavities or ground areas with lower stiffness and strength compared to the natural ground. The detrimental effects of weak zones can include corrosion of tunnel appurtenances, diminished load-carrying capacity due to significant deterioration, and even complete liner failure as the surrounding rock/soil gradually loosens around the weak zone (Helfrich, 1997; Leung and Meguid, 2011; Meguid and Kamel, 2014). Moreover, weak zones can impact the seismic performance of tunnels, and many tunnels are located in earthquake-prone areas. Hence, examining both the static and dynamic behaviour of tunnel liners in the presence of weak zones is imperative to ensure tunnel protection during and after seismic events.

To address above issue, a series of shaking table tests were conducted in this research, introducing weak zones at tunnel crown, shoulder, and spring line positions. Subsequent numerical simulations were performed to explore the detailed influence of weak zones on tunnel and ground response, elucidating their underlying mechanisms.

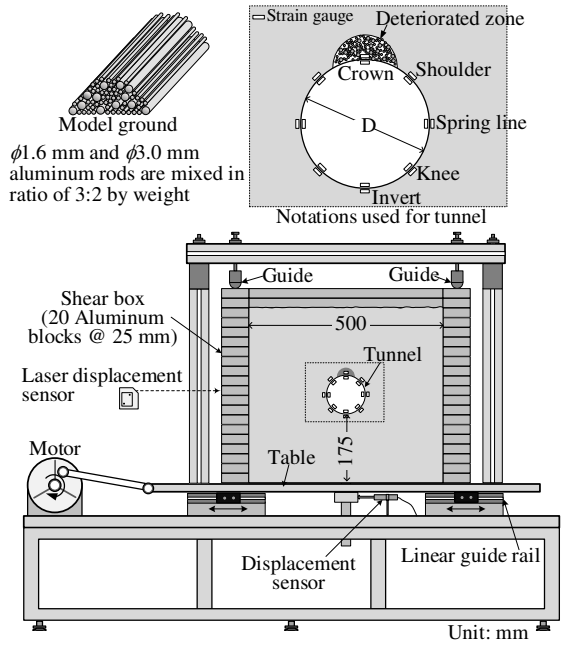

Figure 1. Schematic diagram of the 2D shaking table test apparatus with the tunnel model (Ahmed and Cui, 2022)

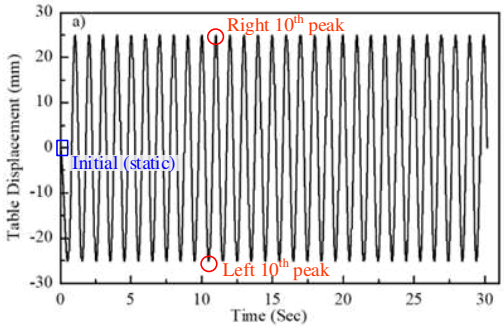

Figure 2. The input wave of the table displacement

2 OUTLINE OF SHAKING TABLE TEST AND CORRESPONDING SIMULATION

2.1 Tunnel model

Figure 1 illustrates the schematic diagram of the 2D shaking table test apparatus alongside the tunnel model. The tunnel was replicated using an acrylic tube with a thickness of 3 mm and an outer diameter of 100 mm, which was scaled down to 1/100 of the actual tunnel. Eight strain gauges were affixed to the lining model to measure the bending moment. Each section was furnished with two strain gauges—one positioned internally and the other externally to the lining structure. The bending moment at the corresponding locations is calculated using these two strain values. The positions of the strain gauges are denoted according to the notation presented in Figure 1. Throughout the experiment, the tunnel model behaved as an elastic material, and no failures occurred.

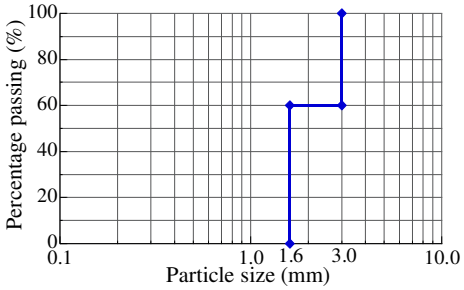

Figure 4. PSD of the ground material

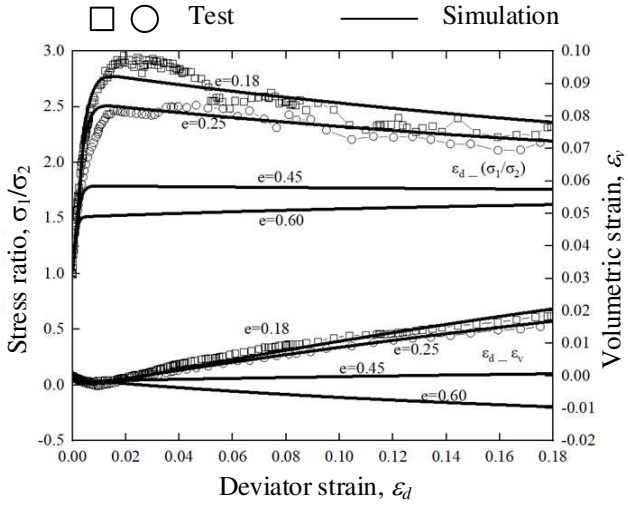

Figure 4. Stress-strain dilatancy relation of aluminium rod mass under biaxial compression test

2.2 Ground material of the surrounding ground and weak zone

The aluminium rods are frequently adopted to investigate the sectional performance of the geo-structure (e.g., Xu et al., 2019), since they simulate granular media like soil in a 2D manner. The experiments were conducted with an overburden ratio of 2.0. During the ground preparation phase, aluminium rods, each with a uniform length of 50 mm, were utilized to represent the soil mass. These roes, with 1.6 and 3.0 mm in diameter, were mixed in a ratio of 3:2 by weight. Figure 3 shows the particle size distribution (PSD), and the unit weight of the ground is 22.3 kN/m3. Biaxial tests were then carried out on the aluminum rod mass to observe stress-strain and stress-dilatancy relationships under constant lateral pressure (σ2=19.6 kPa) for the void ratio of 0.18 and higher void ratio, as illustrated in Figure 4.

Weak zones were induced around the tunnel perimeter by increasing the void ratio at specific locations to mimic field conditions. This was achieved by uniformly removing calculated numbers of aluminium rods, allowing for examination of the effects of the targeted void ratios of 0.45. Further, three tests were conducted, introducing weak zones at

the crown, shoulder, and spring line positions. The weak zone dimensions were maintained at 20 mm above the tunnel surface, resulting in an angle of 51.6 degrees at the tunnel center.

2.3 2D shaking table test apparatus

Typically, a tunnel is much longer in the direction of excavation than its diameter. It is constrained by the surrounding ground at both the front and the rear along this axis, with no longitudinal deformation occurring. Consequently, the behaviour of the tunnel within any given section can be considered two-dimensional. For example, a 2D trapdoor model test apparatus with aluminium rods (Ladanyi and Hoyaux, 1969; Xu et al., 2019) is often used to model the tunnel excavation problem. By inspiring with these apparatus, 2D shaking-table test apparatus, illustrated in Figure 1, was custom-developed for this study (Ahmed and Cui, 2022). This apparatus is capable of acceleration through an electric actuator and precise control via a digital control module. The inner size of the shaking box was 500 mm × 500 mm and comprised 20 parallel aluminium blocks that were 25 mm in height and connected via smooth, movable bearings. These bearings provide frictionless roller supports, facilitating unrestricted horizontal movement. The table can oscillate sinusoidally from 0.5 to 2 Hz, with a maximum displacement of 25 mm from its neutral position. The acceleration and displacement responses of the table were recorded using an acceleration gauge and displacement gauge affixed to the table. For this research, a sinusoidal wave with a frequency of 1 Hz and a shaking duration of 30 seconds was selected as the input wave. The displacement waveform corresponding with the input wave collected by the displacement gauge is depicted in Figure 2.

2.4 Testing procedure and measurements

The soil material was compacted using a tamping rod for each 5 cm height to maintain a constant unit weight and achieve a void ratio of 0.18. The aluminium rods were first set to the height beneath the bottom of the tunnel; then, the tunnel was installed in the prescribed position. Further, the ground at both sides of the tunnel and the overburdened ground were again set using the same method. In scenarios involving weak zones, a precise number of aluminium rods were selectively extracted to simulate these areas. Accuracy in forming the weak zones was ensured by marking the targeted region with a marker and removing the calculated amount necessary to achieve the desired void ratio. Throughout this procedure, particles under lower confining pressure were preferentially removed to prevent disturbance of the surrounding soil.

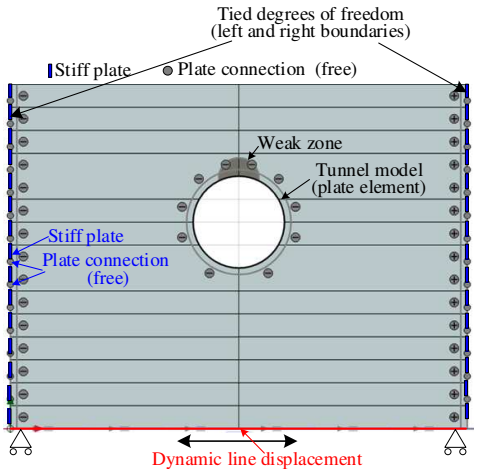

Figure 5. Shaking table test simulation model a) Geometry and boundary conditions

Table 1. Modified cam-clay model parameters

	Surround	Weak
Compression index λ	0.125	
Swelling index κ	0.0075	
The slope of Critical State line *M*	0.46	
Void ratio e	0.77	1.175
Pre-consolidation pressure (kPa)	160	60
Poisson's ratio ν_{ur}	0.25	
Unit weight γ kN/m^3	22.30	18.12
Rayleigh damping coefficient α	8	100
Rayleigh damping coefficient β	2	

Thereafter, the shaking is applied to the table to check the seismic behaviour of the ground and tunnel lining. As mentioned above, the acceleration and displacement of the shaking table and the strain data are collected throughout the experiment, and the sampling frequency is 1,000 values per second. For image capture, the camera orientation was perpendicular to the direction of displacement, and consecutive photos were taken at intervals of 0.01 s. These images were analyzed using the particle image velocimetry (PIV) technique to calculate ground displacement. Subsequently, the volumetric strains were determined based on this displacement.

2.5 Outline of the simulation

The shaking table test was simulated by the finite element program Plaxis 2D, which was widely employed for various geotechnical engineering applications, including deformation, stability, and flow analysis.

Figure 5 depicts the model geometry and boundary conditions. To replicate the shaking of the model, a dynamic line displacement, following the acceleration and displacement time history of the experiment, as shown in Figure 3, was applied at the base of the model. As mentioned earlier, the shaking table consists of 20 pieces of iron blocks, ensuring that the movement or

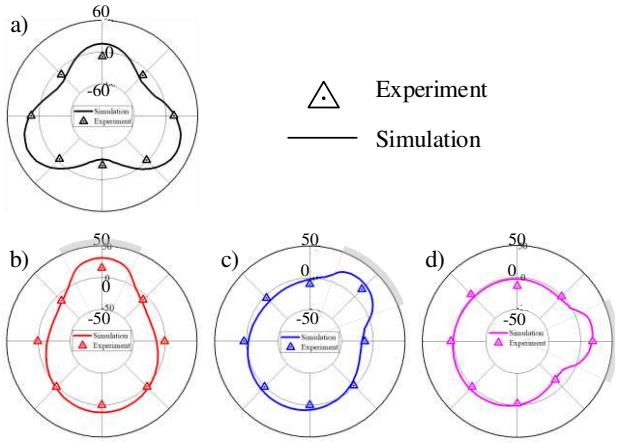

Figure 6. Bending moment distribution before shaking (10^{-3}N·m/m) a)No-weak zone, weak zone at b)crown, c) shoulder d) spring line

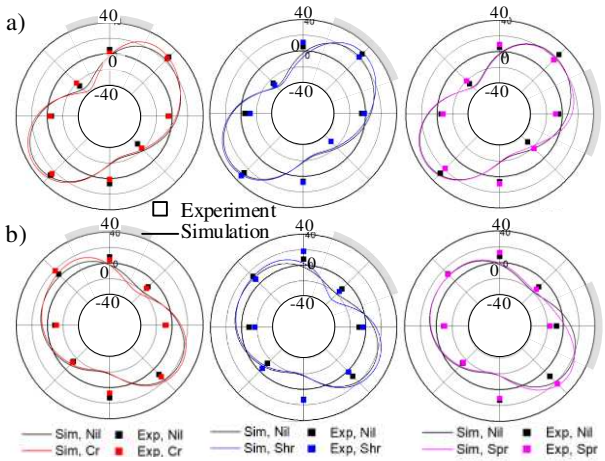

Figure 7. BM due to shaking at the peak displacement of the 10th cycle (10^{-3} N· m/m) a) left peak, b) right peak.

displacement of the ground at the left and right boundaries of the model occurs with the same magnitude and direction. Stiff plates were introduced at the left and right boundaries of the simulation model to model these blocks. A "free plate connection" free from the translation was included between these plates to replicate the same behaviour observed in the experiment.

During shaking in the experiment, the movement or displacement of the ground at the left and right boundaries of the model exhibit identical magnitude and direction, attributed to the structure of the iron blocks supporting the model ground. To replicate this phenomenon, a boundary condition known as "Tied degrees of freedom" was implemented at the left and right boundaries of the model. This condition connects nodes at the same elevation on both boundaries, ensuring they experience identical horizontal displacements (Plaxis 2D Reference Manual, 2022).

The mechanical behavior of the surrounding ground and the weak zone was modelled using the Modified Cam Clay model, with parameters determined by fitting the results of biaxial compression tests, as illustrated in Figure 3. The final parameters are presented in Table 1. The tunnel is modelled as an elastic plate (E = 3.14 GPa), which has the same size (3 mm) and stiffness as the experiment.

3 RESULTS

3.1 Response of the tunnel before shaking

Figure 6 shows the bending moment distribution along the tunnel lining caused by the weak zone at the crown, right shoulder, and right spring lines at static conditions, respectively, obtained from experimental results and corresponding simulation (Ahmed and Cui, 2022). The simulation results match well with the experiment results since a similar bending behaviour can be observed along the tunnel lining at static conditions. Figure 6 a) shows that when a weak zone was placed at the crown, the tunnel bends towards the vicinity of the weak zone at the crown, wherein the maximum bending moment occurs at the crown while the bending moment at the shoulder and spring line slightly bend inwards.

Similarly, as shown in Figure 6 b), when the weak zone was placed at the right shoulder, the tunnel bends towards the vicinity of the weak zone at the right shoulder, wherein the maximum bending moment occurs at the right shoulder while the bending moment at the left shoulder, crown, right spring line, and knee slightly bends inwards. When the weak zone was placed at the right spring line, Figure 6 c) shows that the tunnel bends towards the vicinity of the weak zone at the right spring line, wherein the maximum bending moment occurs at the right spring line while the bending moment at the right shoulder and knee slightly bend inwards. At static conditions, when a cavity or a weak zone is introduced, the tunnel lining tends to bend towards it. This tendency can be due to the smaller stiffness of the weak zone compared to the stiffness of the original surrounding ground, which produces a space for the tunnel lining to bend into when subjected to overburden pressure.

3.2 Response of tunnel during shaking

The tunnel response has been analyzed in terms of bending moment (BM), and a good agreement between experimental and simulation results has been confirmed.

Figure 7 a) illustrates the distribution of BM for the 10th left peak displacement. The simulation results indicate a significant impact of the weak zone on BM

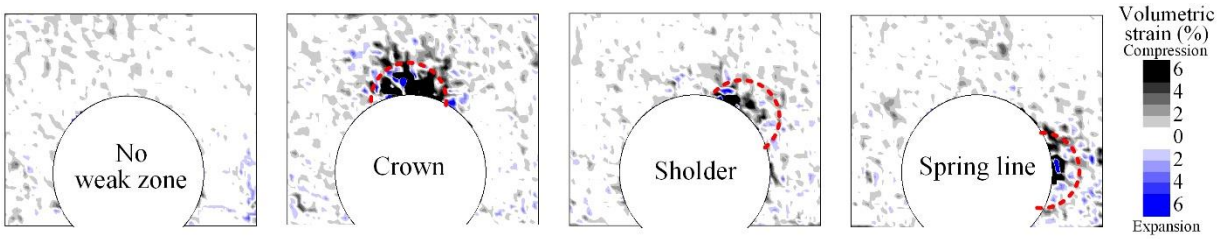

Figure 8. Volumetric strain distribution for 10th right peak displacement observed from experiment

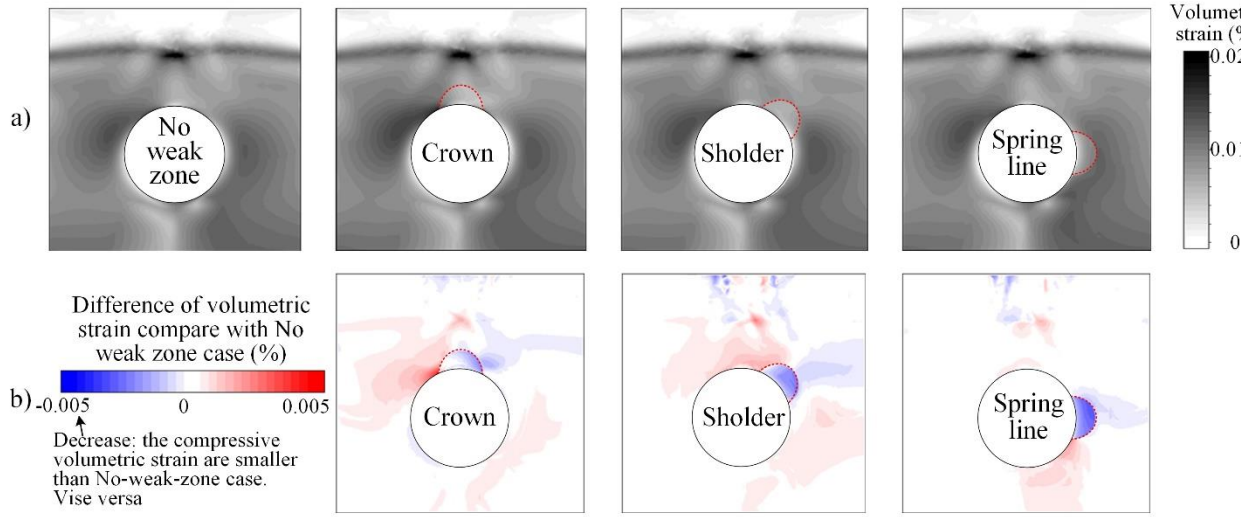

Figure 9. Volumetric strain distribution for 10th right peak displacement calculated by simulation) a) volumetric strain, b) difference from the result of No-weak zone

due to shaking. Compared to the scenario without a weak zone, BM tends to shift towards the weak zone when it is included in the analysis model. Specifically, when the weak zone is positioned at the crown, outward BM between the crown and right shoulder increases, and inner bending amplifies at the left shoulder. Similarly, when the weak zone is situated at the right shoulder, outward BM at the right shoulder increases. Placement of the weak zone at the right spring line results in heightened outward BM at that location. However, this phenomenon was not observed in the experimental results, although some locations along the tunnel exhibit similar correlations between simulation and experiment results.

Similarly, Figure 7 b) presents the BM distribution for the 10th right peak displacement. It is evident that the weak zone significantly influences the BM of tunnel during shaking. When the weak zone is positioned at the crown, outward BM between the crown and left shoulder increases, and inner bending intensifies at the right shoulder. Likewise, with the weak zone placed at the right shoulder, outward BM between the crown and left shoulder increases, and inward BM at the right shoulder rises. When the weak zone is located at the right spring line, outward BM at the right knee increases, while bending at the right spring line tends to shift inward. These phenomena are observable in both the simulation and experimental results. The phenomena observed in the simulation results indicate that the existence of a weak zone around the tunnel lining can cause changes in the bending behaviour of the tunnel when subjected to dynamic movement. When the tunnel bending is directed diagonally towards the right direction, the tunnel tends to bend itself towards the weak zone, which has lesser stiffness than the surrounding ground.

3.3 Response of ground during shaking

Figure 8 illustrates the distribution of volumetric strain corresponding to the 10th right peak displacement observed during the experiment. As previously mentioned, volumetric strain is determined based on ground displacement analyzed from photographs. The figure indicates predominant ground compression induced by shaking, particularly noticeable at the weak zone location, where a localized increase in volumetric strain occurs, likely due to particle transfer into the created voids during shaking. Additionally, an increase in volumetric strain is observed in the neighbouring area of the weak zone, suggesting that the ground's deformation characteristics change with the creation and positioning of the weak zone.

The volumetric strain calculated from simulations is depicted in Figure 9 a). Only compression is observed in the simulation, with volumetric strain showing smaller values compared to the experiment. This difference can be attributed to variations in the weak zone creation process. In the simulation, the weak zone with a high void ratio is initially incorporated into the model ground, and gravity analysis determines the initial state of the ground. Thus, in the simulation, volume strain due to weak zone creation is already accounted for in the initial stage. Consequently, the volumetric strain shown in Figure 8 encompasses deformation resulting from weak zone creation, whereas the volumetric strain from simulation represents only the incremental volume strain due to shaking.

Since the effect of weak zone position on volumetric strain is unclear, differences in volumetric strain compared to the no-weak zone case are plotted in Figure 9 b). This figure mainly focuses on the effect of the position of the weak zone and illustrates changes in volumetric strain distribution by varying the weak zone position.

Observations reveal that when the weak zone is added at the crown or right shoulder, volumetric strain increases in the ground adjacent to the left shoulder and right knee. Placing the weak zone at the right spring line increases volumetric strain in the ground adjacent to the right knee. Notably, volumetric strain increases in the surrounding ground adjacent to sections of the tunnel lining, experiencing outward bending when a weak zone is added. Conversely, volumetric strain decreases near the weak zone, as this area experiences a lesser reaction from the surrounding ground due to lower stiffness. The decreased load is redistributed to the surrounding ground, and as a result, larger volumetric strain occurs on both sides of the weak zone.

4 CONCLUSIONS

This research conducted 2D shaking table experiments and corresponding simulations to assess how weak zones affect the seismic response of circular tunnels. The findings can be summarized as follows:

- As weak zones develop, the ground experiences reduced shear strength, leading to significant deformations. These deformations are significantly influenced by the position of the weak zone relative to the tunnel.
- Under static conditions, the tunnel lining deforms towards the weak zone and inward at neighbouring points, increasing bending moments before shaking. For instance, a weak zone at the shoulder position causes outward deformation at the shoulder and inward displacement at the crown and spring line positions, potentially leading to cracking or complete lining failure.
- During shaking, weak zones induce strains in the groundmass, redistributing deformation characteristics in the surrounding ground. The extent and magnitude of ground strain depend on the position of the weak zone and the duration of shaking. This redistribution of ground deformation destabilizes the support of the tunnel from the surrounding ground, exerting additional bending forces on the tunnel lining.

ACKNOWLEDGEMENTS

The authors are grateful for the financial support provided by JSPS KAKENHI Grant Number 19K04594.

REFERENCES

Ahmed, S., and Cui Y. (2022), Static and dynamic response of circular tunnels with loose cavities behind liner, *Proceedings of ITA-AITES World Tunnel Congress* 2022.

Gomes, R. C., Gouveia, F., Torcato, D., Santos, J. (2015) Seismic response of shallow circular tunnels in two-layered ground, *Soil Dynamics and Earthquake Engineering*, 75, 37–43.

Leung, C., Meguid, M. A. (2011) An experimental study of the effect of local contact loss on the earth pressure distribution on existing tunnel linings, *Tunnelling and Underground Space Technology*, 26 (1), 139–45.

Ladanyi, B. and Hoyaux, B. (1969) A study of the trapdoor problem in a granular mass. *Canadian Geotechnical Journal*. 6(1): 1-14

Meguid, M. A., Dang, H. K. (2009) The effect of erosion voids on existing tunnel linings, Tunnelling and Underground Space Technology, 24 (3), 278–286.

Meguid, M. A., Kamel, S. (2014) A three-dimensional analysis of the effects of erosion voids on rigid pipes. *Tunnelling and Underground Space Technology*, 43, 276–89.

Plaxis, (2022) Connect Edition V22.00 Plaxis 2D-Reference Manual. Bentley Advancing Infrastructure.

Xu, C., Zhang, X., Han, J., Yang, Y. (2019) Two-dimensional soil-arching behavior under static and cyclic loading, *International Journal of Geomechanics,* 04019091.

Zhang, X., Ye, Z., Min, B., Xu, Y. (2019) Effect of voids behind lining on the failure behavior of symmetrical double-arch tunnels, *Symmetry*, 11 (10), 1–16.